Розглянуто механізм формування гексаферит барію з заміщенням іонами Al і Ga. Заміщення відбуваються в підгратці 12k. Це призводить до виникнення нееквівалентних положень іонів Fe^{3+}, і в месбауерівських спектрах з алюмінієм виділяються 7 секстетов, а з галієм 6. Заміщення алюмінієм підвищує коерцитивну силу, а входження галію знижує коерцитивну силу. Визначено кути між магнітним моментом і напрямком γ-випромінювання в досліджувальних составах

Ключові слова: замещенный гексаферит барію, мезбауерівська спектроскопія, намагніченість, коерцитивна сила, температура Кюрі

Рассмотрен механизм формирования гексаферритов бария с замещением ионами Al и Ga. Замещения происходят в подрешетке 12k. Это приводит к возникновению неэквивалентных положений ионов Fe^{3+} и в мессбауэровских спектрах с алюминием выделяются 7 секстетов, а с галлием 6. Замещение алюминием повышает коэрцитивную силу, а для галлия отмечено понижение коэрцитивной силы. Определены углы между магнитным моментом и направлением γ-излучения в исследованных составах

Ключевые слова: замещенные гексаферриты бария, мессбауэровская спектроскопия, намагниченность, коэрцитивная сила, температура Кюри

UDC 535.421; 537.622; 538.91
DOI: 10.15587/1729-4061.2017.91409

STUDY OF THE FEATURES OF THE MAGNETIC AND CRYSTAL STRUCTURES OF THE $BaF^{E}_{12-X}AL_XO_{19}$ AND $BaFe_{12-X}Ga_XO_{19}$ SUBSTITUTED HEXAGONAL FERRITES

V. Kostishyn
Doctor of Physical and Mathematical Sciences, Professor, Head of Department*
E-mail: drvgkostishyn@mail.ru
V. Korovushkin
Doctor of Geological-Mineralogical Scienses, Associate Professor*
E-mail: krvsch@mail.ru
I. Isaev
Engineer*
E-mail: isa@misis.ru
A. Trukhanov
PhD*
E-mail: truhanov86@mail.ru
*Department of Technology for Electronic Materials
National University of Science and Technology "MISiS"
Leninskiy ave., 4, Moscow, Russia, 119049

1. Introduction

The structural and compositional diversity of hexagonal ferrites makes them a convenient object for a research of magnetic and electric properties [1, 2]. The structure of $BaFe_{12}O_{19}$ substituted ferrites, commonly used in technology is similar to $MeFe_{12}O_{19}$ (Me^{2+}–Ba^{2+}, Sr^{2+}, Pb^{2+}, Ca^{2+}) magnetoplumbite mineral, in which the oxygen layers are a set of hexagonal (HCP), and cubic (CCP) packing of hexagonal (R) and spinel (S) blocks containing Fe^{3+} ions [3, 4].

Interest in research of M-type barium ferrites with a hexagonal structure ($BaFe_{12}O_{19}$) and solid solutions is due to their high functional properties. Excellent chemical stability and corrosion resistance make them environmentally safe and usable virtually without restrictions in time. The combination of high coercive force (H_c~160–55 kA/m) [5] and rather high residual induction provides permanent magnets with satisfactory specific magnetic energy, and their low conductivity (ρ~10^8 ohm·cm) allows applying hexaferrite magnets in the presence of high-frequency magnetic fields.

2. Literature review and problem statement

Barium ferrite is isostructural with $PbFe_{12}O_{19}$ magnetoplumbite mineral [6], the crystal structure type of which has been first determined by Adelskold in 1938. The anisotropy energy constant of hexaferrites is by two orders of magnitude greater than that of garnet-type ferrites, which has paved the way for practical applications: permanent magnets, magnetic recorders and microwave equipment [7, 8]. Hexagonal ferrites have been successfully used in the decimeter and centimeter electromagnetic radiation absorption field (electromagnetic compatibility of microelectronic devices and radio equipment, "STEALTH" technology and so on). Previous research of hexagonal barium ferrite showed that it is an insulator, in which Kramers-Anderson short-range indirect exchange between the magnetoactive iron ions through oxygen anion prevails, i. e., the pair exchange integral depends on the valence angles and interatomic distances in Fe–O–Fe bonds [9]. Strong sublattice exchange in bonds causes collinear ferrimagnetic alignment with the Curie temperature of ~740 K [10]. The functional properties of ferrites can be controlled by changing the number of mag-

netic couples of iron ions, for example, introducing diamagnetic Al, Sc, Ga and In ions. Depending on the doping degree and temperature, the solid solutions formed undergo phase transitions accompanied by different types of alignment.

Hexaferrites contain only Fe^{3+}ions as magnetoactive, which are localized at the nodes having octahedral ($4f_2$, 2a, 12k), tetrahedral ($4f_1$) and bipyramidal (2b) oxygen environment [6].

Isomorphous substitution in the crystal structure of hexagonal Ba ferrites is essential in the formation of their magnetic and electric properties. Isomorphous elements are often Sr^{2+} and Ca^{2+} cations, which substitute some Ba^{2+} ions, and weak-magnetic or non-magnetic In^{3+}, Sc^{3+}, Al^{3+}, Ga^{3+} cations, etc. substitute Fe^{3+} ions. Non-magnetic cations lead to breakage of exchange coupling between Fe^{3+} ions, thus changing the magnetic characteristics of the ferrite [9].

However, the issues remain about localization of both divalent and trivalent ions in the structure due to the presence of 5 structural positions in hexaferrites, as well as the cation distribution impact on the magnetic and electric properties. The isomorphous substitution in hexagonal and spinel blocks may cause the angular magnetic structure. Thus, in [10], the authors believe that the angular magnetic structure at the Al entry into the hexaferrite lattice occurs at x=~3. However, the issues of how various elements influence the noncollinearity angle, in what positions substitution occurs and at what element contents are not fully understood. The ability of Mössbauer spectroscopy to determine the angle θ between the magnetic moment in the hexaferrite and the γ-radiation direction with the known direction of the crystallographic axis C allows solving this problem.

3. The purpose and objective of the research

The research aim was to determine the localization of isomorphic Al and Ga impurities in the hexagonal M-type barium ferrite structure and the effect of these impurities on the magnetic properties of the ferrite.

The research objectives included:

– determining the substituted hexaferrite sintering temperature;

– determining the structural positions of the Fe ions substitution with impurity ions;

– determining the magnetic parameters (specific and residual magnetization, coercive force, hysteresis loop shape) in the source barium hexaferrite compared to the substituted one;

– determining the angle θ between the magnetic moment and the γ-radiation direction in isotropic and anisotropic hexaferrites by analyzing the intensity ratio of resonance lines in the Mössbauer spectra.

4. Materials and methods of researching the substituted hexaferrites

The research objects were samples of polycrystalline M-type $BaFe_{12}O_{19}$ hexaferrite in the powder form, polycrystalline $BaFe_{12-x}Al_xO_{19}$ in the d=0.1 mm foil form and polycrystalline $BaFe_{11,4}Ga_{0,6}O_{19}$. The samples have been prepared of Fe_2O_3, Me_2O_3 oxides, and $BaCO_3$ carbonate according to the known ceramic technique in appropriate proportions:

$$BaCO_3+5.7Fe_2O_3+xMe_2O_3=BaFe_{12-x}Me_xO_{19}+CO_2.$$

The initial composition was subjected to air synthesizing calcination at 1200 °C (6 h) and then sintered at 1300 °C (6 h). After sintering, the sample was slowly cooled in the furnace (~100 °C/h).

Mössbauer spectroscopy, X-ray radiography, and magnetic measurements were used to examine the features of the crystal structure, composition and properties. Mössbauer studies were performed on the Ms1104-Em spectrometer and the spectra were processed by the Univem Ms program (Russia, Southern Federal University, Rostov-on-Don). The measurements were performed at room temperature (300 K) for powders and foil. The isomer shift was determined relative to α-Fe. X-ray diffraction patterns were obtained on the DRON-3M apparatus in CuK_α radiation. Magnetic parameters such as saturation magnetization σ_s, coercive force H_c, residual magnetization σ_r, hysteresis loop shape and area were measured by the VS M 250 vibration magnetometer in the 20 kOe magnetic field at 300 K.

5. The results of studying the substituted barium hexaferrites

X-ray phase analysis of $BaFe_{12}O_{19}$ samples after annealing at 1100, 1150 and 1200 and 1300 °C was held in order to determine the phase formation kinetics of substituted hexaferrites. It was found that hexaferrite with magnetoplumbite-type structure, isostructural with $BaFe_{12}O_{19}$ was present in the samples as the main phase (>91 %) after annealing at 1100 °C. The presence of an impurity phase – $BaFe_2O_4$ was observed. In addition to the main phase ($BaFe_{12}O_{19}$), the presence of a second phase – $Ba_2Fe_6O_{11}$ was noted after annealing at 1150 °C. The $BaFe_2O_4$ impurity phase was detected after annealing at 1200 °C (Fig. 1).

$BaFe_{12}O_{19}$ hexaferrite without intermediate phases was found at the sintering temperature of 1300 °C.

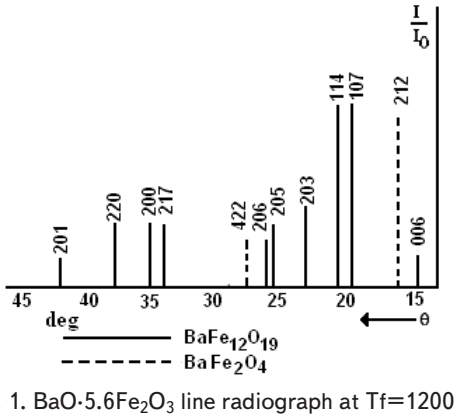

Fig. 1. $BaO{\cdot}5.6Fe_2O_3$ line radiograph at Tf=1200 °C

The high-temperature X-ray radiography revealed that $BaFe_{12}O_{19}$ is formed in two stages:

at t=700–900 °C $BaCO_3+6\ Fe_2O_3\rightarrow$

$\rightarrow BaFe_2O_4+5\ Fe_2O_3+CO_2\uparrow$;

at t=900–1200 °C $BaFe_2O_4+5\ Fe_2O_3=BaFe_{12}O_{19}$.

At the same time, other intermediate phases may be formed during the second stage [11]. The formation mechanism and the sintering temperature of polycrystalline aluminum- and gallium-substituted barium hexaferrite are similar.

Mössbauer spectra of $BaFe_{12}O_{19}$ and $BaFe_{12-x}Al_xO_{12}$ substituted ferrite samples in powder and foil forms are shown in Fig. 2, *a*. Table 1 shows the parameters of Mössbauer spectra after decomposition.

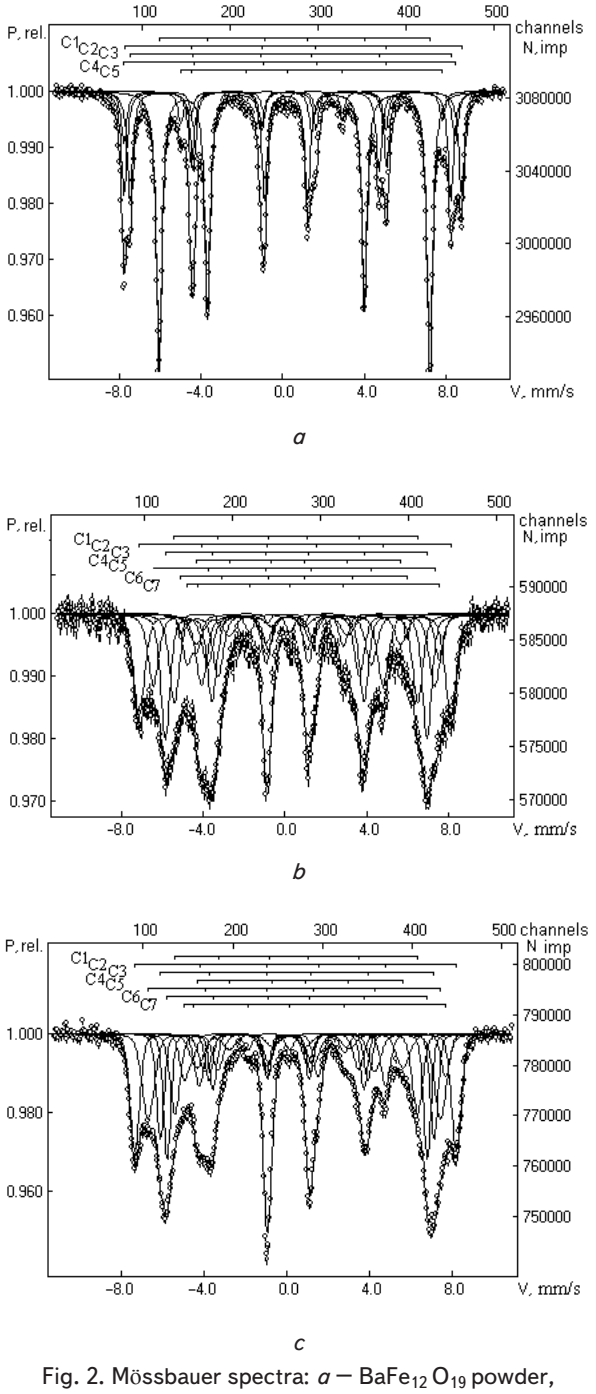

Fig. 2. Mössbauer spectra: *a* – $BaFe_{12}O_{19}$ powder, *b* – $BaFe_{12-x}Al_xO_{19}$ powder, *c* – $BaFe_{12-x}Al_xO_{19}$ foil

The Mössbauer spectrum decomposition model was based on the physical sense, visual spectrum resolution, achievement of minimum χ^2 and minimum discrepancy between the experimental spectrum and the model.

To study the magnetic properties of substituted hexaferrites, their saturation magnetization, residual magnetization, coercive force, Curie temperature and hysteresis loops in comparison with the unsubstituted hexaferrite were measured. Fig. 3 shows hysteresis loops of $BaFe_{12}O_{19}$ (Fig. 3, *a*) and $BaFe_{9,9}Al_{2,1}O_{19}$ (Fig. 3, *b*) ferrites, and Table 2 – their magnetic characteristics.

Table 1

Mössbauer parameters of the samples: $BaFe_{12}O_{19}$ powder, $BaFe_{12-x}Al_xO_{19}$ powder, $BaFe_{12-x}Al_xO_{19}$ foil

Sample, material	Sublattice, spectral component	Isomer shift δ, mm/s	Quadrupole splitting Δ, mm/s	Magnetic fields at Fe^{57} nuclei H, kOe	Component areas S, %
Isotropic $BaFe_{12}O_{19}$, powder	12k-C1$(Fe^{3+})_{VI}$	0.35	0.42	414	49.9
	2a-4$(Fe^{3+})_{VI}$	0.33	0.00	507	8.8
	$4f_1$-C3$(Fe^{3+})_{IV}$	0.26	0.22	491	18.6
	$4f_2$-2$(Fe^{3+})_{VI}$	0.39	0.20	516	17.6
	2b-C5$(Fe^{3+})_{V}$	0.29	2.21	400	5.1
Isotropic $BaFe_{12-x}Al_xO_{19}$, powder	$12k^1$-C1$(Fe^{3+})_{VI}$	0.31	0.38	370	18.0
	$4f_2$-C2$(Fe^{3+})_{VI}$	0.37	0.13	474	22.9
	12k-C3$(Fe^{3+})_{IV}$	0.31	0.43	397	23.2
	2a-C4$(Fe^{3+})_{VI}$	0.37	0.52	311	8.3
	$4f_1$-C5$(Fe^{3+})_{IV}$	0.28	0.24	428	16.6
	$4f_1^1$-C6$(Fe^{3+})_{IV}$	0.22	0.37	345	2.6
	2b-C7$(Fe^{3+})_{V}$	0.29	2.1	383	8.4
Aniso-tropic $BaFe_{12-x}Al_xO_{19}$, foil	12k-C1$(Fe^{3+})_{VI}$	0.29	0.39	396	25.8
	$4f_2$-C2$(Fe^{3+})_{VI}$	0.37	0.13	485	17.4
	$4f_1$-C3$(Fe^{3+})_{IV}$	0.25	0.32	423	14.8
	2a-C4$(Fe^{3+})_{VI}$	0.37	0.52	312	6.8
	$4f_1^1$-C5$(Fe^{3+})_{IV}$	0.27	0.02	449	12.3
	$12k^1$-C6$(Fe^{3+})_{IV}$	0.26	0.32	366	13.8
	2b-C7$(Fe^{3+})_{V}$	0.29	2.21	400	8.9

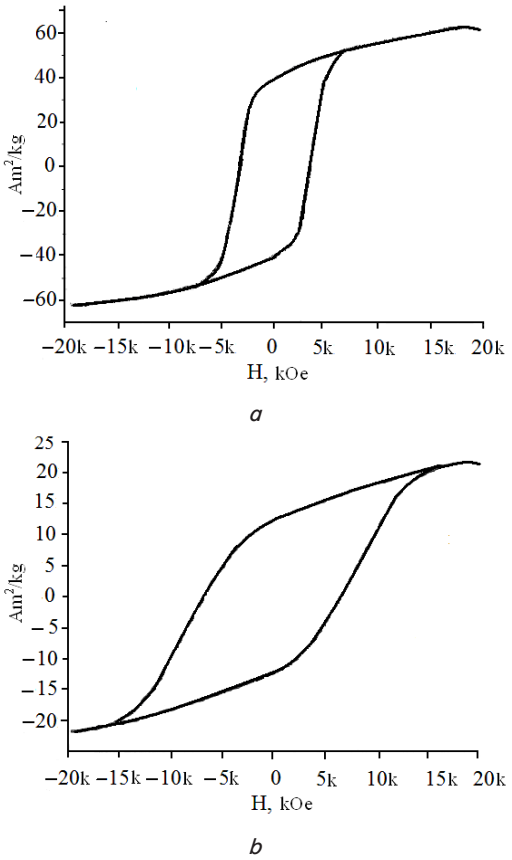

Fig. 3. The hexagonal ferrites hysteresis loops: *a* – $BaFe_{12}O_{19}$, *b* – $BaFe_{9,9}Al_{2,1}O_{19}$

Table 2

Magnetic properties of $BaFe_{12}O_{19}$, $BaFe_{9,9}Al_{2,1}O_{19}$ and $BaFe_{11.4}Ga_{0,6}O_{19}$ hexagonal ferrites

Ferrite	Specific saturation magnetization σ_s, Am^2/kg	Specific residual magnetization, σ_r, Am^2/kg	Coercive force H_c, kA/m	Curie temperature, K
$BaFe_{12}O_{19}$	64.61	40.13	273	720
$BaFe_{9,9}Al_{2,1}O_{19}$	21.68	12.13	532	543
$BaFe_{11.4}Ga_{0,6}O_{19}$	37.10	23.17	246	620

The effect of Ga dopants on magnetic properties depending on the localization in the hexagonal barium ferrite structure was examined in the $BaFe_{11.4}Ga_{0,6}O_{19}$ sample. Fig. 4 shows a Mössbauer spectrum of the sample, taken at K 300, and Table 3 – the Mössbauer parameters.

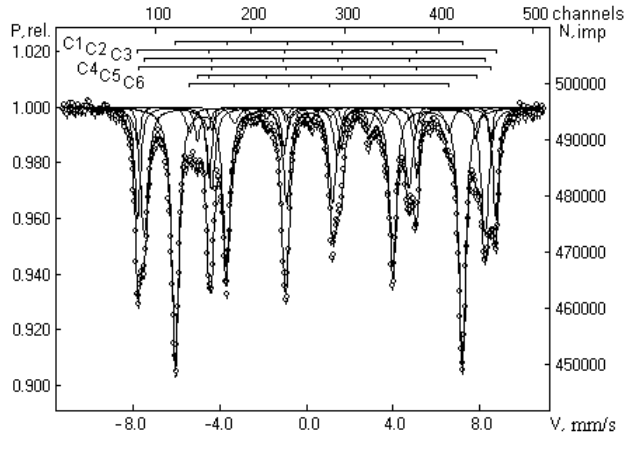

Fig. 4. The $BaFe_{11.4}Ga_{0,6}O_{19}$ sample Mössbauer spectrum

Table 3

Mössbauer parameters of $BaFe_{11.4}Ga_{0,6}O_{19}$ substituted ferrite

Sample, material	Sublattice, spectral component	Measured shift δ, mm/s	Quadrupole splitting Δ, mm/s	Magnetic field at Fe^{57} nuclei H, kOe	Component areas S, %
Isotropic $BaFe_{11.4}Ga_{0,6}O_{19}$ powder	12k-C1$(Fe^{3+})_{VI}$	0.35	0.41	411	47.6
	$4f_2$-C2$(Fe^{3+})_{VI}$	0.38	0.20	512	16.3
	$4f_1$-C3$(Fe^{3+})_{IV}$	0.27	0.21	487	24.2
	2a-C4$(Fe^{3+})_{VI}$	0.34	-0.02	505	4.3
	$12k^1$-C5$(Fe^{3+})_{IV}$	0.35	0.44	370	3.0
	2b-C7$(Fe^{3+})_{V}$	0.29	2.21	400	4.6

Unlike spectra of hexaferrites with Al, the $BaFe_{11.4}Ga_{0,6}O_{19}$ hexaferrite spectrum was decomposed into 6 sextets. The additional sextet was designated as $12k^1$ and assigned to the 12k sublattice.

The magnetic characteristics of $BaFe_{11.4}Ga_{0,6}O_{19}$ are also of interest. Fig. 5 shows the magnetic hysteresis loop for this sample, and Table 2 – the magnetic characteristics.

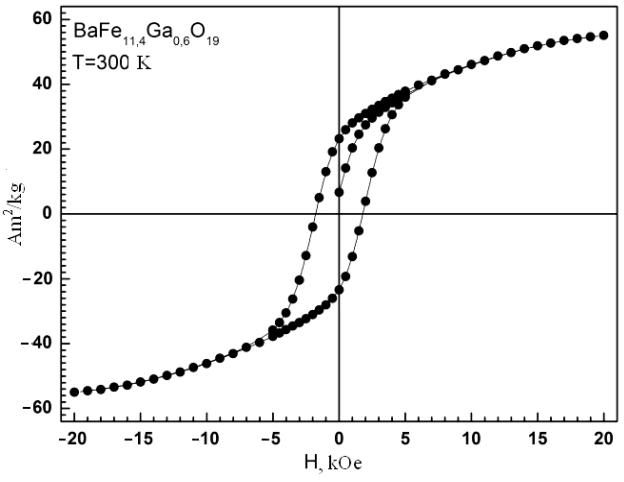

Fig. 5. The $BaFe_{11.4}Ga_{0,6}O_{19}$ sample hysteresis loop

Spontaneous magnetization was determined from the field dependence of the linear extrapolation to zero field.

6. Discussion of the results of studying $BaFe_{12-x}Al_xO_{19}$ and $BaFe_{12-x}Ga_xO_{19}$ hexaferrites

The analysis of the $BaFe_{12}O_{19}$ sample spectrum (Fig. 2, *a*) shows that it is a superposition of five sextets corresponding to 12k, $4f_1$, $4f_2$), 2a, 2b sublattices. The occupancies of sublattices correspond to their theoretical values for the hexagonal structure M, 12:4:4:2:2, respectively. The Mossbauer spectra parameters for iron ions, localized in these sublattices coincide with the data obtained in [11].

Satisfactorily decomposition of Mössbauer spectra of $BaFe_{12-x}Al_xO_{12}$ substituted hexaferrite into 5 sextets proved impossible. The best option was the spectrum decomposition into 7 sextets, corresponding to 12k, $12k^1$, $4f_1$, $4f_2$, $4f_1^1$ 2a and 2b sublattices. The emergence of $12k^1$ and $4f_1^1$ sublattices is associated with the Al^{3+} localization features and 12k and $4f_1$ division into two. Comparison of the sextets areas (Table 1) allows concluding that Al^{3+} ions are localized mainly in 12k positions, resulting in allocation of 7 sextets in the spectrum. If, according to the $BaFe_{12}O_{19}$ ferrite formula, 50 % rel., falling to 6 Fe^{3+}ions should theoretically be in the 12k sublattice, then 41.2 % accounts for iron ions of the 12k sublattice in $BaFe_{12-x}Al_xO_{19}$ isotropic ferrite, while the occupancy change in other sublattices is within the error. Proceeding from the 12k sublattice occupancy, the crystal-chemical formula for $BaFe_{12-x}Al_xO_{19}$ powder will be $BaFe_{9,9}Al_{2,1}O_{19}$.

When analyzing the Mössbauer spectra parameters (Table 1), we can note a decrease in the values of magnetic fields at Fe^{57}nuclei in almost all sublattices, and not only for the 12k sublattice. Indeed, indirect exchange interactions between Fe^{3+} ions of different Fe(12k)–O–Fe($4f_2$), Fe(12k)–O––Fe(2b), Fe($4f_2$)–O–Fe(2b) Fe(12k)–O–Fe($4f_1$) and Fe(12k)–O–Fe(12k) sublattices occur in the hexaferrite structure. Therefore, the Fe^{3+}–Al^{3+} substitution in the 12k sublattice leads to the breakage of magnetic coupling with other sublattices and, consequently, to a decrease in magnetic fields at Fe^{57} nuclei. If the H_{eff} dependence is performed as

$4f_2$>2a>$4f_1$>12k>2b in the unsubstituted hexaferrite, then in the substituted isotropic hexaferrite due to the different number of exchange couples of 12k with other sublattices – $4f_2$>$4f_1$>12k>2b>2a. In addition, the isomer chemical shift in the substituted hexaferrite is markedly reduced for Fe^{3+} ions of all sublattices as compared with the unsubstituted hexaferrite. This is probably due to the covalence increase of Fe^{3+} ions bond, with a decrease in the unit cell parameter, since the ionic radius rAl^{3+}_{VI} (0.051 nm) is less than rFe^{3+}_{VI} (0.064 nm).

The $BaFe_{9,9}Al_{2,1}O_{19}$ powder Mössbauer spectrum showed slight signs of texture because it satisfied the peak intensity ratio $3_{1\text{-}6}$:$2_{2\text{-}5}$:$1_{3\text{-}4}$ equal to 3:2.11:1.18 and the angle θ, determined from the expression $A_{1\text{-}6}/A_{2\text{-}5}=3(\cos^2\theta)/4(\sin^2\theta)$, is 53.9°. These values are quite close to the ratio of 3:2.2:1.1 in polycrystals at the angle θ=55°.

The integral intensity ratios, characteristic of polycrystals are not satisfied in the spectrum of hexaferrite foil with isomorphic aluminum. So, the most appropriate foil sample decomposition was carried out by setting 7 sextets at the intensity ratio of 3:1.39:1.13. Such intensity ratio is characteristic of the samples with a certain degree of texture. According to the obtained ratio, the deflection angle of the magnetic moments from the γ-radiation wave vector θ is 44.6°. Based on the results, we can say that hexagonal Ba ferrites in the foil form have an evident texture. The foil sample Mössbauer spectrum, taken at 87 K showed the worst peak resolution from Fe^{3+} ions of different sublattices than at 300 K, which is explained by opposite directions of spins of Fe^{3+} ions of structural sublattices. The angle θ remained almost unchanged, being 44.2°.

Breakage of Fe–O–Fe magnetoactive couples between hexaferrite sublattices leads both to a reduction in local magnetic fields at Fe^{57}nuclei, the emergence of non-equivalent 12k and $4f_1$ nodes, and a change in the magnetic characteristics. Fig. 3 shows the $BaFe_{12}O_{19}$ and $BaFe_{9,9}Al_{2,1}O_{19}$ ferrite hysteresis loops, and Table 2 – their magnetic characteristics.

Table 2 shows that the exchange coupling weakening decreases the Curie temperature by 177 degrees, the specific saturation magnetization by 43 Am^2/kg compared with the $BaFe_{12}O_{19}$ ferrite. The hysteresis loops show a significant squareness decrease and area increase compared to the unsubstituted Ba hexaferrite. At the same time, the hexaferrite coercive force increased almost 2-fold. This result can be essential when choosing hard-magnetic materials for non-metallic permanent magnets.

The analysis of the $BaFe_{11.4}Ga_{0,6}O_{19}$ ferrite spectrum showed, unlike $BaFe_{9,9}Al_{2,1}O_{19}$ hexaferrite, minor differences in the isomer shift and quadrupole splitting for all sublattices compared with the unsubstituted hexaferrite, but the magnetic field decrease from 2 to 4 kOe is observed for all sublattices, except 2b. More substantial changes occur in the areas of all spectral components, except $4f_2$. The area reduction from Fe^{3+} ions of 12k, 2a and 2b sublattices indicates entry of Ga ions into them. Additional sextet, labeled $12k^1$, was assigned to the 12k sublattice, as their isomer shift and quadrupole splitting values are similar. Reduction of magnetic fields at Fe^{57} nuclei is due to the iron ions being surrounded with nonmagnetic Ga ions and breakage of its magnetic couples.

The analysis of magnetic characteristics showed (Fig. 5) that the hysteresis loop does not go into a state of magnetic saturation even in magnetic fields of up to 20 kOe, which can be explained by the intralattice exchange interaction weakening. The maximum specific magnetization in 20 kOe fields was 55.04 Am^2/kg. The data (Table 2) show that gallium doping (x=0.6) of $BaFe_{12}O_{19}$ hexaferrite leads to a decrease in almost all magnetic parameters. The spontaneous magnetization decreased by 27.5 Am^2/kg, residual magnetization by 17 Am^2/kg, coercive force by 27 kA/m, Curie temperature by 100 K. This confirms that the substitution of iron ions with diamagnetic gallium ions reduces the number of magnetic neighbors of iron ions and, as a consequence, leads to an earlier failure of long-range magnetic order when samples are heated. The comparison of barium hexaferrites doped with various metals shows that gallium doping makes the material magnetically softer in relation to $BaFe_{12}O_{19}$, and aluminum doping – magnetically harder. A complete dependence of the magnetic condition of $BaFe_{12}O_{19}$ hexaferrite on doping with different elements can be observed on their quantitative composition dependences, which is planned in further work.

7. Conclusions

1. It is shown that hexagonal Ba ferrite formation occurs in several stages via intermediate phases. $BaFe_2O_4$ intermediate phase with a spinel structure and $Ba_2Fe_6O_{11}$ intermediate phase with orthorhombic structure are formed in the 1100–1200 °C sintering temperature range. Formation of $BaFe_{12}O_{19}$ hexaferrite with magnetoplumbite-type structure starts at 1200 °C and ends at 1300 °C.

2. It is found that the Fe–Al substitution in $BaFe_{9,9}Al_{2,1}O_{19}$ hexaferrite occurs mainly in the 12k sublattice, whereby the 12k and $4f_1$ sublattices are divided into two. The Fe – Ga substitution in $BaFe_{11,4}Ga_{0,6}O_{19}$ hexaferrite occurs in the 12k sublattice, as well as in the 2a and 2b sublattices, and only the 12k sublattice is divided into two.

3. Measurements of magnetic characteristics of $BaFe_{9,9}Al_{2,1}O_{19}$ and $BaFe_{11,4}Ga_{0,6}O_{19}$ hexaferrites showed that substitution of Fe^{3+} ions with Al^{3+} and Ga^{3+} leads to a decrease in specific saturation magnetization, residual magnetization, and Curie temperature. It is shown that the Al (x=2.1) entry into the lattice increases the coercive force from 273 to 532 kA/m, increasing the hexaferrite magnetic hardness, and the Ga entry lowers the coercive force and reduces the magnetic hardness. The rate of changes in the magnetic parameters depends on the degree of substitution of Fe^{3+}ions.

4. The angle θ between the magnetic moment and the γ-radiation direction in isotropic and anisotropic hexaferrites was determined by analyzing the intensity ratio of resonance lines in the Mössbauer spectra. The deflection angle of the magnetic moments from the γ-radiation wave vector θ for the substituted hexaferrite in the foil form is 44.6°, indicating the occurrence of texture. The $BaFe_{9,9}Al_{2,1}O_{19}$ powder Mössbauer spectrum showed no texture, as it showed the intensity ratio of 3:2.11:1.18 and the angle θ is equal to 53.9°.

The research is performed under the Research Task No. 11.2502.2014/K on 17.07.2014 within the project part of the state task in the field of scientific activity (Subject No. 3219022).

References

1. Tsutaoka, T. Magnetic phase transitions in substituted barium ferrites $BaFe_{12-x}$(Ti0.5Co0.5)xO19 (x=0–5) [Text] / T. Tsutaoka, N. Koga // Journal of Magnetism and Magnetic Materials. – 2013. – Vol. 325. – P. 36–41. doi: 10.1016/j.jmmm.2012.07.050
2. Erenstein, W. Multiferroic and magnetoelectric materials [Text] / W. Eerenstein, N. D. Mathur, J. F. Scott // Nature. – 2006. – Vol. 442, Issue 7104. – P. 759–765. doi: 10.1038/nature05023
3. Tokunaga, Y. Multiferroic M-Type Hexaferrites with a Room-Temperature Conical State and Magnetically Controllable Spin Helicity [Text] / Y. Tokunaga, Y. Kaneko, D. Okuyama, S. Ishiwata, T. Arima, S. Wakimoto et. al. // Physical Review Letters. – 2010. – Vol. 105, Issue 25. doi: 10.1103/physrevlett.105.257201
4. Tan, G. Structure and multiferroic properties of barium hexaferrite ceramics [Text] / G. Tan, X. Chen // Journal of Magnetism and Magnetic Materials. – 2013. – Vol. 327. – P. 87–90. doi: 10.1016/j.jmmm.2012.09.047
5. Trukhanov, A. V. Crystal structure and magnetic properties of the $BaFe_{12-x}AlxO_{19}$ (x=0.1–1.2) solid solutions [Text] / A. V. Trukhanov, V. O. Turchenko, I. A. Bobrikov, S. V. Trukhanov, I. S. Kazakevich, A. M. Balagurov // Journal of Magnetism and Magnetic Materials. – 2015. – Vol. 393. – P. 253–259. doi: 10.1016/j.jmmm.2015.05.076
6. Seifert, D. Synthesis and magnetic properties of La-substituted M-type Sr hexaferrites [Text] / D. Seifert, J. Topfer, F. Langenhorst, J.-M. Le Breton, H. Chiron, L. Lechevallier // Journal of Magnetism and Magnetic Materials. – 2009. – Vol. 321, Issue 24. – P. 4045–4051. doi: 10.1016/j.jmmm.2009.07.088
7. Harris, V. G. Recent advances in processing and applications of microwave ferrites [Text] / V. G. Harris, A. Geiler, Y. Chen, S. D. Yoon, M. Wu, A. Yang et. al. // Journal of Magnetism and Magnetic Materials. – 2009. – Vol. 321, Issue 14. – P. 2035–2047. doi: 10.1016/j.jmmm.2009.01.004
8. Harris, V. G. Modern Microwave Ferrites [Text] / V. G. Harris // IEEE Transactions on Magnetics. – 2012. – Vol. 48, Issue 3. – P. 1075–1104. doi 10.1109/tmag.2011.2180732
9. Trukhanov, A. Evolution of structure and physical properties in al-substituted Ba-hexaferrites [Text] / A. Trukhanov, L. Panina, S. Trukhanov, V. Turchenko, M. Salem // Chinese Physics B. – 2016. – Vol. 25, Issue 1. – P. 016102. doi: 10.1088/1674-1056/25/1/016102
10. Kamzin, A. S. Surface magnetism of Al-substituted hexagonal ferrites of the type Sr-M [Text] / A. S. Kamzin, L. P. Olkhovyk // FTT. – 1999. – Vol. 41, Issue 10. – P. 1806–1813.
11. Kostishyn, V. G. Influence of the technological factors and chemical composition on the thermostability and electromagnetic properties of the M-type hexaferrites [Text] / V. G. Kostishyn, V. G. Andreev, N. D. Ursuljak, A. G. Nalogin, D. N. Citanov, A. V. Timofeev et. al. // Surface. X-ray, synchrotron and neutron investigations. – 2015. – Issue 12. – P. 68–73. doi: 10.7868/s0207352815120100